Novel Asymmetric IPM Rotor Design Using Cascaded Multiphysics Topology Optimization

Mohamed Reda Mahmoud, *Member, IEEE*, Mohamed N. Ibrahim, *Senior Member, IEEE*, and Peter Sergeant, *Senior Member, IEEE*

***Abstract*—Sustainable motor design is crucial for improving energy efficiency and reducing material consumption. This paper introduces a novel asymmetric interior permanent magnet (IPM) rotor design using topology optimization (TO). The study employs a two-stage TO approach to design IPM rotor. In the first stage, a multi-objective electromagnetic TO is conducted to enhance the average torque and reduce the mass of the magnetically active rotor zone. In the second stage, structural TO is performed to minimize the mass of the magnetically inactive rotor zone while maintaining mechanical integrity, ensuring the rotor withstands operational mechanical stresses. The asymmetric topology-optimized IPM (ATO-IPM) machine is analyzed and benchmarked against the conventional IPM design and the symmetric topology-optimized IPM (STO-IPM) design. The results indicate that the asymmetric flux barriers enhance the torque performance. The ATO-IPM design offers significantly more efficient utilization of permanent magnets (PMs) and improved torque density by approximately 13.3% compared to the conventional IPM motor. Moreover, ATO-IPM design supports the advancement of sustainability by improving efficiency by 2.3% compared to conventional design. Furthermore, ATO-IPM designs save about 46.7% of the amount of silicon steel of the conventional topology.**

***Index Terms*—Asymmetric design, Finite element analysis (FEA), Interior permanent magnet (IPM) machine design, Multi-objective optimization, Solid isotropic material with penalization (SIMP), Topology optimization.**

I. Introduction

Eco-design is a vital approach to achieving sustainability in the field of electrical machines. Eco-design, which incorporates environmental considerations into the design phase, strives to reduce the ecological imprint of electric machines during their entire life cycle [1]. Key eco-design requirements embrace improving energy efficiency, which reduces operational energy consumption and greenhouse gas emissions, minimizing material use, and using recyclable materials to assist end-of-life recovery [2].

Among electric machines, the interior permanent magnet (IPM) configurations have become a cornerstone in high-performance applications such as electric vehicles (EVs) and industrial automation, owing to their superior torque density, high efficiency, and extended field-weakening capabilities [3]. Moreover, IPM machines are extensively utilized due to their superior mechanical stability and reduced susceptibility to permanent magnet (PM) demagnetization compared to surface-mounted PM (SPM) topology [4]. However, it is important to further enhance their performance because IPM machines rely on rare-earth PM, which is costly and has detrimental environmental impacts. Therefore, enhancing torque production efficiency and maximizing the utilization of magnetic materials are critical research objectives. One of the key factors limiting the torque capability of conventional symmetric IPM machines lies in their torque production characteristics. The existing symmetric IPM machines have a current angle offset of around 45 electrical degrees between the peak of PM and reluctance torque components. Consequently, the maximum resultant torque can utilize only a fraction of the available PM and reluctance torque components, which decreases the use of both components in the maximum resultant torque [5]. To overcome this limitation, a novel IPM design approach, defined as asymmetric IPM (AIPM), is adopted by shifting the peak positions of the two torque components closer to each other. This alignment improves the utilization ratios of torque components and increases the maximum resultant torque [6].

Recently, AIPM rotor topologies have emerged as a promising strategy for improving torque characteristics. In [7], an AIPM design considered a combination of rare-earth PM and ferrite PM to enhance the torque characteristics and improve the PM utilization. The work [8] proposed an IPM motor with hybrid layer PM configuration to improve the torque performance by enhancing the magnetic field shifting (MFS) utilization. The AIPM topology improved both the torque density and torque ripples simultaneously. Ref. [9] proposed an asymmetric rotor topology for a PM-assisted

Manuscript received December 03, 2025; revised February 28, 2026, April 12, 2026, and April 21, 2026; accepted April 30, 2025. Date of publication June 25, 2026. Date of current version May 27, 2026.

Mohamed Reda Mahmoud is with the Department of Electromechanical, Systems, and Metal Engineering, Ghent University, Gent 9052, Belgium, also with FlandersMake@UGent— Corelab MIRO, Leuven 3001, Belgium, and also with the Department of Electrical Engineering, Minia University, Minia 61111, Egypt (e-mail: Mohamed.Reda@ugent.be or Mohamed. Hassan@mu.edu.eg).

Mohamed N. Ibrahim is with the Department of Electromechanical, Systems, and Metal Engineering, Ghent University, Gent 9052, Belgium, also with FlandersMake@UGent— Corelab MIRO, Leuven 3001, Belgium, and also with the Department of Electrical Engineering, Kafrelshiekh University, Kafr el-Sheikh 33511, Egypt (e-mail: Mohamed.Ibrahim@ugent.be).

Peter Sergeant is with the Department of Electromechanical, Systems, and Metal Engineering, Ghent University, Gent 9052, Belgium, also with FlandersMake@UGent— Corelab MIRO, Leuven 3001, Belgium (e-mail: Peter.Sergeant@ugent.be).

(*Corresponding Author*: *Mohamed Reda Mahmoud*)

Digital Object Identifier 10.30941/CESTEMS.2026.00018

synchronous reluctance motor with position-biased magnets to enhance the overall performance in terms of efficiency, torque ripple, and average torque. Moreover, a novel asymmetric rotor pole for a wound-field synchronous machine was introduced in [10] to achieve low torque ripple and high saliency ratio. The work [11] introduced a novel AIPM rotor by combining V-shape and spoke PM configurations. The design used the MFS to maximize the average torque by minimizing the angle between the PM and reluctance torque components. In [12], a novel AIPM machine is proposed, in which asymmetric V-shaped PMs are integrated with outer flux barriers. This configuration enables a substantial increase in torque compared with a conventional V-shaped IPM machine while maintaining the same PM volume. However, the previous work improved the performance of the IPM machine; it depends on the experience of the designer. Further, it is important to optimize the motor design to efficiently utilize the rare-earth PM and maximize the performance [13].

Traditional electric machine design optimization methods typically use parameter-based optimization algorithms, i.e., the parametric sweep, to find geometric variables within set constraints [14]. However, such approaches are limited by manufacturing restrictions and the developer experience integrated in the chosen parameterization. Dimensional optimization is the commonly used approach to calculate the dimensions, such as the magnet thickness or the magnet length, to optimize the IPM machine design [15]. However, the dimensional optimization of the IPM motor design has limitations, such as the flux barriers that control the PM leakage flux. To address these limitations, topology optimization (TO) offers an alternative optimization methodology with a high degree of freedom [16]. Moreover, TO plays a crucial role in designing a new generation of electric machines. TO is a powerful design methodology that facilitates the optimal distribution of materials, such as air, silicon steel, and PMs, within a specified design space [14]. TO promises unique solutions to find the equilibrium between the eco-design aspects, i.e. enhancing the machine performance and reducing the amount of the required material to build these machines [17].

TO was originally developed for solid mechanical design, but it has recently been used to design electromagnetic applications, i.e., electric machines [14]. However, applying TO for electric machine design is still a developing approach. In literature review, TO has been employed to address several critical issues in the design of IPM machines. Several TO techniques, such as ON/OFF [18] or bidirectional evolutionary structural optimization (BESO) [19]-[20], level set or topological derivative [21]-[22], and density-based methods [23], have been suggested for the magnetic-only TO of IPM rotors. In [16], TO was performed to enhance the torque performance of IPM machines by optimizing the rotor domain. However, this study applied TO to design half the area of one pole and use the symmetric property, which prevents the algorithm from generating asymmetric designs. Further, the flux barrier shape of the V-shape IPM motor was optimized using TO by considering flux barrier symmetry, which limits the TO ability to optimize the design [24]. Additionally, TO was applied with a large degree of freedom to design a complete one-pole, allowing asymmetric results [25]. However, the structural strength of the optimized design was not considered. Moreover, a density-based TO was applied with a high degree of freedom to maximize the average torque of a permanent magnet synchronous motor (PMSM) [26]. However, the study considered only one rotor position during the TO process. Moreover, the structural strength of the design and overall performance were not considered for the optimized design.

Most of the electric machine designs proposed through TO were electromagnetically designed. However, TO has been applied considering structural phenomena for magnetic devices. In [27], a structural TO was performed on the magnetic actuator design to minimize the mechanical compliance of the armature, in addition to maximizing the developed force between the armature and yoke. Furthermore, the structural TO was applied to minimize the rotor mass of a high-speed IPM motor used in an electric vehicle while ensuring sufficient mechanical strength [28].

From the previous literature review, it is important to maximize the performance of the IPM machines to achieve efficient utilization of rare-earth PM. Further, AIPM had been proposed considering only parametric optimization. Moreover, the TO considered in the literature review was considered to have only a limited degree of freedom by considering symmetric designs. This paper presents a novel asymmetric IPM rotor design using TO. In this study, a cascaded magneto-structural Multiphysics TO will be performed to design the rotor of the IPM motor. The study will introduce both symmetrical and asymmetric designs. The first TO stage is a multi-objective magnetic TO that maximizes the average torque and minimizes the rotor mass. The second stage is performing structural TO to minimize the rotor mass while ensuring acceptable mechanical characteristics. Further, the different TO designs will be analyzed and compared to the conventional design in terms of magnetic flux distribution, torque characteristics, losses, and efficiency.

This article is organized into six sections. Section II presents the conventional design analysis and problem statement. In Section III, the TO process will be introduced. The TO designs and post-processing are illustrated in Section IV. A comparative study for the overall performance analysis of the different designs is presented in Section V. Finally, the outcomes of this study are summarized in Section VI.

II. Conventional Design and Optimization Problem

A. Conventional Design Analysis

Fig. 1 presents the cross-sectional view of the conventional IPM motor structure, which will be considered as the baseline motor for comparative analysis. The main specifications of the IPM motor are illustrated in Table I. The stator has 36 slots with 8 poles, three-phase distributed winding, arranged as shown in Fig. 1. The rotor has eight permanent magnet poles with barriers.

The conventional IPM was optimized in [29] using the parametric response surface method to maximize the torque. In the baseline IPM rotor, the bridge (rib) thickness is 1 mm, which is relatively conservative and leads to reduced torque capability. Reducing the rib to 0.5 mm preserves sufficient mechanical strength, as shown in Fig. 2. Von Mises stress analysis at 5000 r/min verifies that the modified design remains structurally robust. The reduced rib configuration will be considered as a modified design and will be incorporated into comparative analysis, besides the conventional and topology optimized designs, in Section IV. Moreover, the first stage (electromagnetic TO) for the magnetically active zone of the rotor will consider a thickness of 0.5 mm around the rotor outside the design domain of the TO process to provide sufficient mechanical strength.

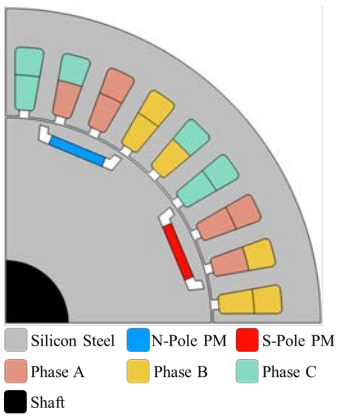

Fig. 1. Cross-sectional view of the conventional IPM motor.

TABLE I
THE MAIN SPECIFICATIONS OF THE IPM MOTOR

Parameter	Value
Rated power/W	450
Rated speed/(r/min)	750
Stator outer diameter/mm	131
Stator inner diameter/mm	86
Axial length of the motor/mm	50
No. of poles	8
No. of stator slots	36
No. of coils per phase	696
Airgap length/mm	0.3
Current density/(A/mm^2)	5
PM width/mm	12
PM thickness/mm	2

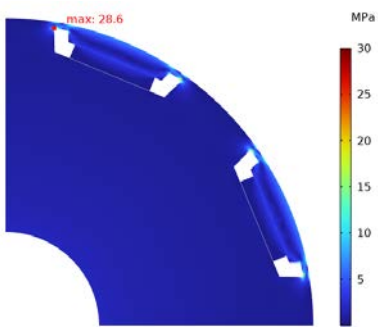

Fig. 2. The von Mises stress of the modified design considering reduced ribs of 0.5 mm.

B. *Optimization Problem*

The design described in Fig. 1 and Table I will be considered the initial design in this study. First of all, the initial design was analyzed. Fig. 3(a) presents the magnetic flux density chart at the rated operating point, which reports low flux densities near the shaft and high flux densities around the permanent magnet.

By separating the magnetic flux density chart into two charts, as shown in Figs. 3(b) and 3(c). Fig. 3(b) presents regions with flux densities lower than 0.5 T (magnetically non-active region). Fig. 3(c) presents regions with flux densities higher than 0.5 T (magnetically active region). Based on this separation, it is clear that the magnetically inactive region is significantly used for mechanical purposes, and the electromagnetic performance of the motor is heavily affected by the region surrounding the magnets.

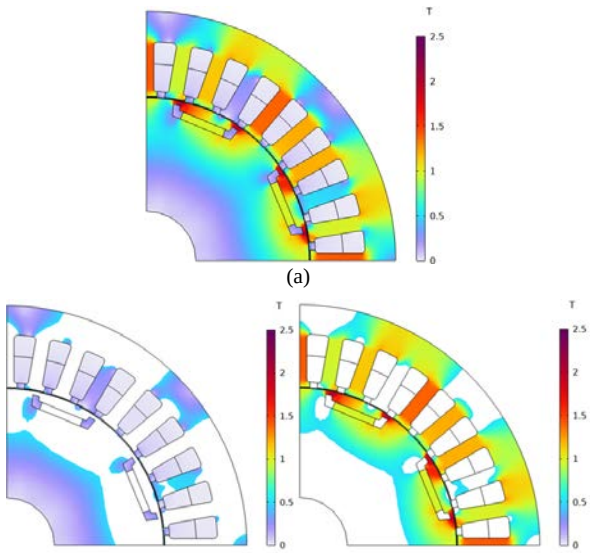

(a)

(b) (c)

Fig. 3. Conventional IPM motor magnetic flux density charts. (a) The complete chart. (b) Chart for flux densities lower than 0.5 T. (c) Chart for flux densities higher than 0.5 T.

The design idea will consider improving the electromagnetic performance, i.e., maximizing the average torque, by performing electromagnetic TO for the magnetic active region. Then, structural TO is applied for the magnetically inactive region to obtain a sustainable design by minimizing the rotor mass.

III. TO FOR IPM MOTOR

In this section, the TO design tool used to design the IPM motor will be presented in detail. This section is divided into three subsections. The density-based TO will be presented in detail in subsection *A*. Then, the IPM motor design process will be formulated in subsection *B*. Finally, the TO results will be presented in subsection *C*.

A. *Density-based TO*

The proposed design domain is divided into cells, which are the same as finite element analysis (FEA). The density-based TO is a gradient-based method that uses a continuous

design variable. A material density (ρ) is used as a design variable, ranging $0 \le \rho \le 1$. Cells with a density $\rho = 0$, are air or void material, and a cell with a density $\rho = 1$ is filled with solid material, i.e., silicon steel. On the other hand, the design variable with densities $0 < \rho < 1$ refers to a material with different properties; i.e., relative permeability is changed between air and that of the silicon steel, and this is called an intermediate material [30]. The intermediate material should be avoided as it has no physical meaning, but it is important to solve the gradient-based optimization problem [31].

The design variable is used to interpolate the material in terms of relative permeability for magnetic TO and Young's modulus for structural TO. In this study, a solid isotropic material with penalization (SIMP) is applied to interpolate the material. The relative permeability ($\mu_{r,e}$) of the ferromagnetic material of each element during solving magnetic TO can be expressed as (1) [32]:

$$\mu_{r,e}\left(\rho_e\right) = \mu_o + \left(\mu_r - \mu_o\right)\rho_e^P \tag{1}$$

where μ_o is the relative permeability of air; P is the penalization factor $P > 1$, which forces the intermediate densities to either 0 or 1. If P is selected to be larger, the intermediate material is subjected to greater penalties and then deleted. Furthermore, the Young's modulus of each element (E_e) is interpolated for structural TO by SIMP as (2):

$$E_e\left(\rho_e\right) = E_o\rho_e^P \tag{2}$$

where E_o is the Young's modulus of the solid ferromagnetic material. Using the design variable directly in the material interpolation step will cause material oscillation. To overcome the oscillatory nature of the material, two processes—filtering and projection—must be implemented ahead of material interpolation.

In this study, the Helmholtz partial differential equation (PDE) filtering function is implemented to smooth the material distribution. The filtered material density ($\tilde{\rho}$) can be expressed as (3) [33]:

$$-R_h^2\nabla^2\tilde{\rho} + \tilde{\rho} = \rho \tag{3}$$

where R_h is the filter radius, which depends on the mesh size within the design domain, and ∇^2 is the Laplace operator. However, the filtering process will introduce more intermediate materials. To mitigate this, the filtered density ($\tilde{\rho}$) should pass through another step called material projection. The projection step improves the boundaries between the ferromagnetic material and air within the design domain by converting the filtered density ($\tilde{\rho}$) into a more discrete form (ferromagnetic material or air). The hyperbolic tangent projection scheme is used as the projection scheme as (4) [34]:

$$\hat{\rho} = \frac{\tanh\left(\beta\eta\right) + \tanh\left(\beta\left(\tilde{\rho} - \eta\right)\right)}{\tanh\left(\beta\eta\right) + \tanh\left(\beta\left(1 - \eta\right)\right)} \tag{4}$$

where $\hat{\rho}$ is the projected density; β is the sharpness parameter; η is the threshold level. The design variable transition between void and solid material can be represented by the hyperbolic tangential projection scheme under different values for the sharpness parameter, as shown in Fig. 4.

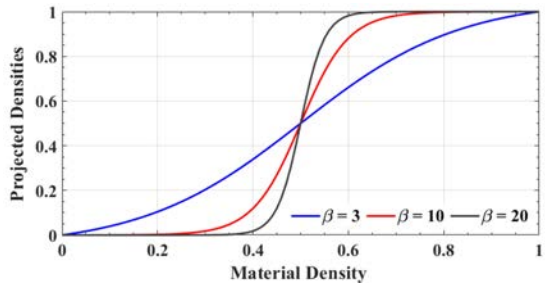

Fig. 4. Hyperbolic tangent projection function shape with η = 0.5 and different values of the sharpness parameter.

B. IPM Motor Design Problem

This subsection will present the design process of the IPM motor using density-based TO. The TO will be applied to design two different rotors. The first is toward symmetrical rotor design by considering half a pole as the design domain and using sector symmetry to assign the material to the second half pole, as shown in Fig. 5(a). The second considers a high degree of freedom with a complete pole as the design domain, as shown in Fig. 5(b). However, all the features of the density-based TO and the FEA are the same for both rotor design processes.

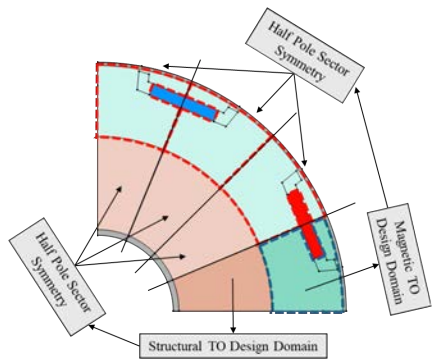

(a)

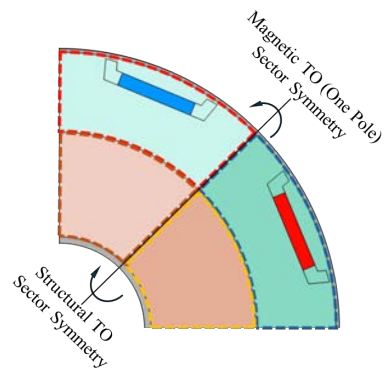

(b)

Fig. 5. Proposed design domains for both magneto and structural TO stages. (a) Symmetrical design. (b) Asymmetric design.

The design process of each configuration is divided into two stages. The first stage is magneto-TO for magnetically active regions, as shown in Fig. 5. The second stage is structural-TO for magnetically inactive regions. The flow chart of the design process is presented in Fig. 6.

1) Magneto-TO

This stage is concerned with improving the electromagnetic performance of the IPM motor in terms of maximizing the average torque (T_{ave}); moreover, minimizing the rotor mass. So, it is a multi-objective magneto-TO for both cases, as (5):

$$\text{Maximize } T_{ave} - w_f \int_{\Omega_1} \rho_e d\Omega_1$$
$$\text{Subject to (s.t.)} \begin{cases} 0 \le \rho \le 1 \\ 0.7V_{\Omega_1} \le V_{opt} \le 0.95V_{\Omega_1} \end{cases} \quad (5)$$

where w_f is a weighting factor; Ω_1 is the design domain surface during magnetic TO; V_Ω is the volume of the design domain, and V_{opt} is the optimal design volume. The optimal design volume is kept between 70% to 95% of the conventional design to ensure acceptable mechanical properties for the magnetically active region. Moreover, an outer ring with a thickness of 0.5 mm is kept outside the design domain to ensure mechanical strength for the magnetically topology-optimized zone.

As illustrated by the flow chart, shown in Fig. 6, the electromagnetic model is solved using FEA at different rotor positions. Then, the objective function and constraints are evaluated. Afterward, the sensitivity analysis is performed using the adjoint variable method (AVM). The problem is solved using the method of moving asymptotes (MMA) to update the design variable [35]. Finally, the material is represented by the density-based TO through filtering, projection, and material interpolation.

2) Structural-TO

Toward sustainable designs, the materials usage must be reduced or efficiently used. Assuming unidirectional operation of the AIPM motor, TO is applied to the magnetically inactive region of the magnetically optimized design. The objective function of structural-TO is to minimize the rotor mass with a constraint for mechanical properties. To ensure acceptable structural strength, the total elastic strain energy ($W_{s,tot}$) is kept lower than the maximum value, which depends on the ferromagnetic material, which prevents the deformation. The structural-TO can be formulated, for both cases, as (6):

$$\text{Minimize } \int_{\Omega_2} \rho_e d\Omega_2$$
$$\text{s.t.} \begin{cases} 0 \le \rho \le 1 \\ W_{s,tot} \le W_{s,max} \end{cases} \quad (6)$$

where Ω_2 is the design domain surface during structural-TO, and $W_{s,max}$ is the maximum value for the total elastic strain, i.e., the value of the conventional design or lower. Then, the structural-TO is performed according to the flow chart shown in Fig. 6. Similar to magneto-TO, both MMA and AVM will be used to solve the structural-TO.

Both the magnetic TO and structural TO are solved in COMSOL Multiphysics version 6.4 using MMA as the optimization algorithm and AVM for sensitivity analysis. The design processes are implemented according to the flowchart shown in Fig. 6. The IPM motor is magnetically analyzed using FEA at different rotor positions in accordance with the slot periodicity of the machine. In this study, the rotor position varies within the range of 0° to 15°. The objective function and constraints are then evaluated. The TO algorithm computes the design variables and updates the material distribution until convergence of the magnetic TO. Afterwards, the structural TO is applied to the magnetically optimized design.

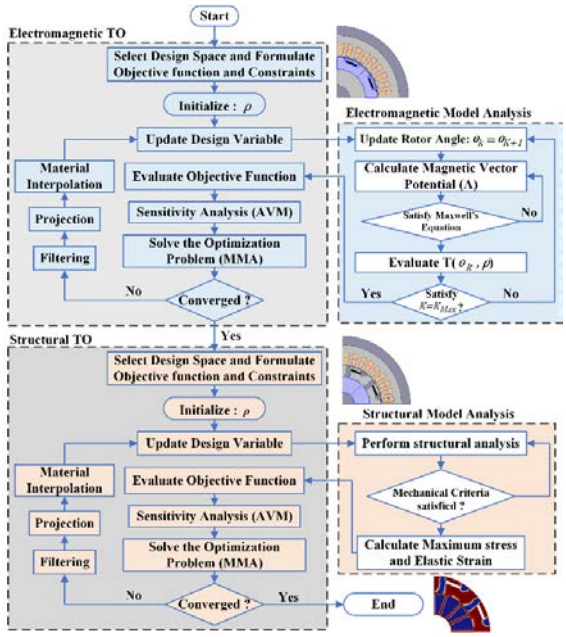

Fig. 6. Cascaded Multiphysics magneto-structural TO design flow chart.

IV. Topology Optimized Designs and Post-Processing

Before performing the design processes, both the magnetic and mechanical properties of the materials are illustrated in Fig. 7 and Table II. Fig. 7 presents the *B-H* characteristics of the silicon steel material (NGO M-36) used in this study. During the magnetic-TO stage, the nonlinearity of the *B-H* characteristics of the ferromagnetic material was considered by calculating the relative permeability iteratively based on Fig. 7.

TABLE II
MECHANICAL PROPERTIES OF THE MATERIALS

Material	NGO M-36	PM
Young's modulus/GPa	190	160
Density/(kg/m^3)	7500	7500
Poisson ratio	0.3	0.24

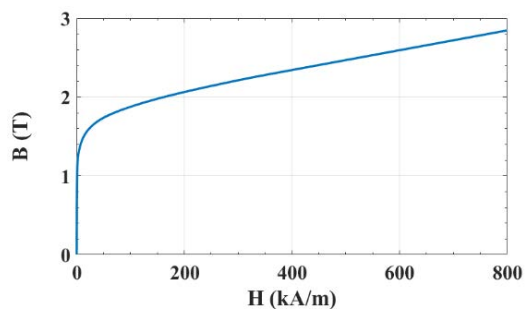

Fig. 7. *B-H* characteristics of silicon steel NGO M-36.

Before applying the TO process, it is important to introduce the parameters of the density-based TO. The parameters of the material representation steps—filtering, projection, and material interpolation, applied in this study, are illustrated in Table III. The filter radius is dependent on the mesh element. Moreover, the number of design variables, which depend on the mesh elements, is illustrated in Table IV.

TABLE III
DENSITY-BASED TO MATERIAL REPRESENTATION STEPS PARAMETERS

Parameter	Symbol	Value
Penalization factor	P	5
Filter radius	R_h	$\frac{r}{2\sqrt{3}}$
Sharpness parameter	β	10
Projection threshold level	η	0.5

where r is the maximum element size of the FEA mesh.

TABLE IV
DESIGN VARIABLES OF THE TO PROCESSES

TO process	Number of design variables
Symmetric magnetic TO	176
Asymmetric magnetic TO	363
Symmetric structural TO	105
Asymmetric structural TO	219

A. TO Results

Before running the algorithm, the initial material densities had been considered 0.5 at iteration 0, as shown in Figs. 8 and 9 for both symmetric and asymmetric magnetic TO, respectively. Afterwards, the algorithm updates the material density at each cell between 0 and 1 to achieve the balance between the objectives and constraints. As presented in Figs. 8 and 9, the algorithm starts to create the magnetic circuit by optimizing the flux barriers to reduce the saturated regions and push the flux to cross the airgap to improve the torque performance. The material distribution varies with high rates after running the algorithm, which will reflect on the convergence curve. Then, the algorithm improves t he boundaries between the different materials till they converge.

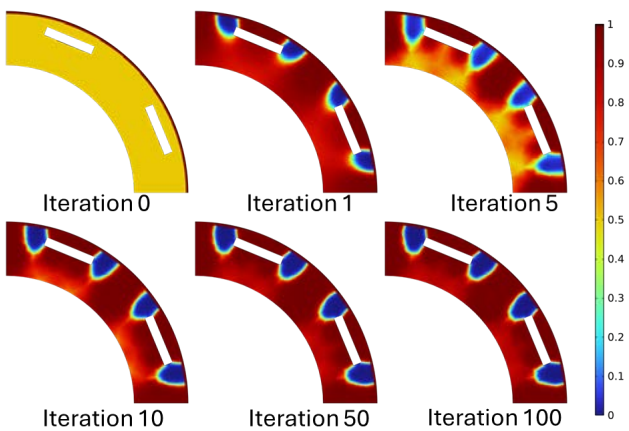

Fig. 8. Material density distribution of symmetric magnetic-TO at different iterations.

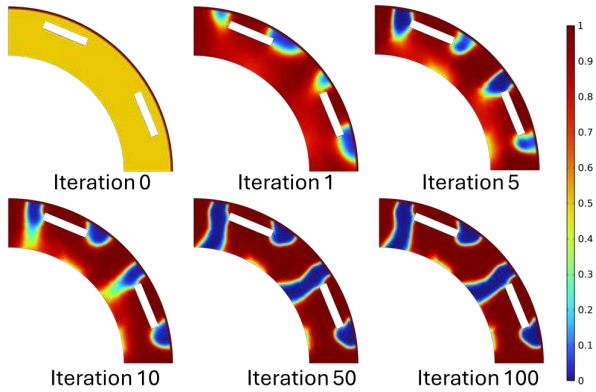

Fig. 9. Material density distribution of asymmetric magnetic-TO at different iterations.

The output geometry of the symmetric magnetic-TO process is presented in Fig. 10 along with magnetic flux lines. The optimal design of asymmetric magnetic TO is presented in Fig. 11. Notably, the asymmetric barriers force the flux lines to cross the air gap and reduce the leakage flux compared to the symmetric design, as shown in Figs. 10(b) and 11(b). Afterward, these geometries are used as an input for the structural-TO, which will be performed to optimize the magnetically inactive zone of the rotor.

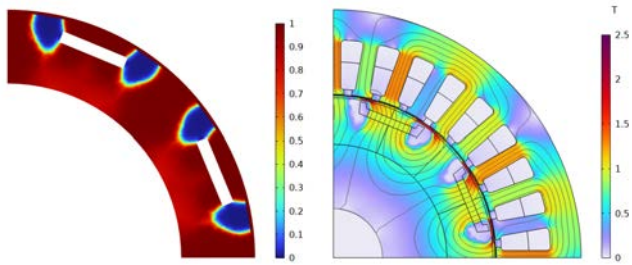

(a) (b)

Fig. 10. Magnetic-TO results of the symmetric design. (a) Material distribution for the magnetically active zone. (b) Magnetic flux density.

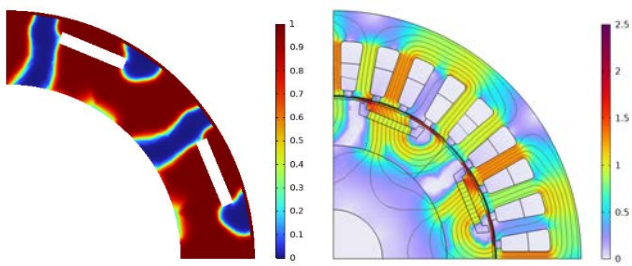

(a) (b)

Fig. 11. Magnetic-TO results of asymmetric design. (a) Material distribution for the magnetically active zone. (b) Magnetic flux density.

For the structural-TO, the structural model is solved at five times the rated speed to ensure sufficient mechanical strength through the operating range. Moreover, the direct contact between the rotor and the shaft must be solid to ensure a reliable mechanical connection between the rotor and the shaft. So, a solid ring around the shaft is kept outside the structural-TO design domain, as shown in Fig. 5. The structural-TO optimal material distribution for the magnetically inactive rotor zone is presented in Fig. 12.

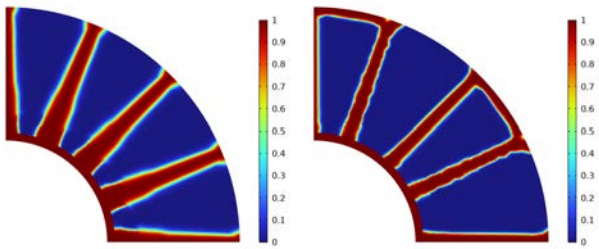

(a) (b)

Fig. 12. Structural-TO results. (a) Material distribution for symmetric topology-optimized IPM (STO-IPM). (b) Material distribution for asymmetric topology-optimized IPM (ATO-IPM).

From the optimization perspective, it is important to discuss the convergence characteristics and computation time. The convergence is defined as the iterative relative change in the design variable. Fig. 13 presents the convergence curves of both magnetic TO processes, where both symmetric and asymmetric cases converge after initial rapid changes, with the symmetric case showing smoother behavior and fewer oscillations. The convergence curves of the structural TO processes are shown in Fig. 14. In contrast, the structural TO results show stronger fluctuations in the early iterations, particularly for the asymmetric case, indicating higher sensitivity to material redistribution. To have a closer look at the computational efficiency, Table V presents the computation time of each TO process. The processor of the computer used for simulation is Intel(R) Xeon Gold 6248R CPU@3.00 GHz, 2 processors, 48 cores with installed memory of 192 GB. The results indicate that magnetic TO requires significantly longer computation time than structural TO because the FEA for magnetic TO considered solving at different rotor positions between 0 to 15°. Moreover, the asymmetric TO requires more computation time than the symmetric TO. However, the difference between the computation time of both magnetic TO is not long because it includes the FEA time required at each iteration.

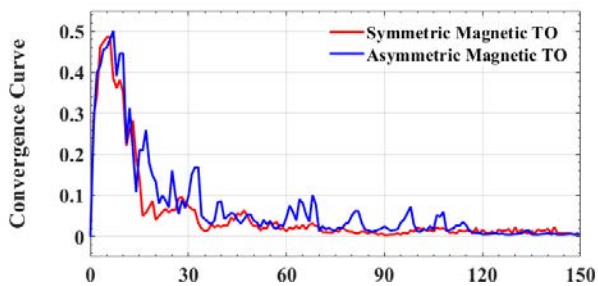

Fig. 13. Convergence curves of magnetic-TO.

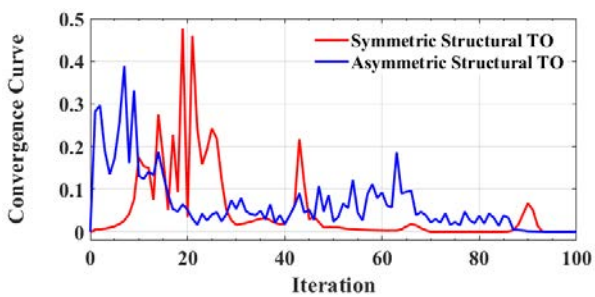

Fig. 14. Convergence curves of structural-TO.

TABLE V
COMPUTATION TIME OF TO PROCESSES

TO process	Number of iterations	Computation time
Symmetric magnetic TO	150	5 h 15 min 24
Asymmetric magnetic TO	150	5 h 27 min 33 s
Symmetric structural TO	100	3 min 12 s
Asymmetric structural TO	100	6 min 8 s

B. Post-processing and Mechanical Analysis

The material density distribution of two stages of magneto-structural TO designs, shown in Fig. 15, contains intermediate material between solid material and air. To obtain an optimal design with boundaries between ferromagnetic material and air, which follows the TO results, post-processing is required. This process is crucial as density-based TO is a gradient-based optimization that uses continuous design variables, which will affect the results. For example, the relative permeability or Young's modulus has different values between that of solid material and air. The post-processing is done by selecting a contour of density 0.5 to form the boundaries between the silicon steel and the air. The areas where densities $\rho < 0.5$ are considered as air, and the areas where densities $\rho \geq 0.5$ are considered as silicon steel (laminations). The optimal designs of the topology-optimized IPM motors are presented in Fig. 16.

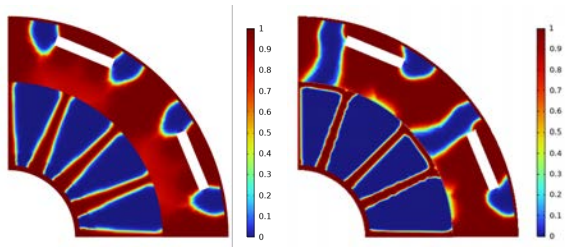

(a) (b)

Fig. 15. Material distribution for magneto-structural topology optimized rotor. (a) STO-IPM motor. (b) ATO-IPM motor.

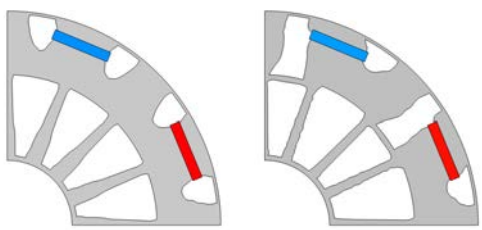

(a) (b)

Fig. 16. Post-processed topology optimized geometries. (a) STO-IPM motor. (b) ATO-IPM motor.

Up to this point, the optimized geometry has been post-processed. It is important to check the mechanical strength of the designs. As it was calculated during the TO process, the Young's modulus of the intermediate material is different from that of the post-processed design. During the TO process, air is modelled as a very small value of Young's modulus, while practically it is a deformed domain. The von Mises stress of the post-processed designs, at 5000 r/min of the motors, is shown in Fig. 17, which validates sufficient mechanical strength for the topology-optimized geometries. However, the von Mises stress of the topology optimized

design is higher than the modified design. This increase is primarily due to the asymmetric material distribution introduced by the TO and the higher local mass concentration, which slightly increases centrifugal effects in certain regions. Despite this, the maximum stress in all designs remains below the allowable limit of the rotor material, ensuring safe operation. Moreover, the topology-optimized designs promise a light mass, which leads to lower moments of inertia (J), which improves the dynamic response of the motor. This can be explained by the electromechanical governing equation, which can be expressed as (7):

$$\frac{\mathrm{d}\omega}{\mathrm{d}t}=\frac{1}{J}\left(T_{\mathrm{e}}-T_{\mathrm{l}}\right) \tag{7}$$

where $\mathrm{d}\omega/\mathrm{d}t$ is the acceleration; T_{e} is the developed electromagnetic torque; T_{l} is the load torque. So, the reduction in the inertia results in high acceleration. Likewise, during deceleration, when (T_{e} − T_{l}) is negative, a smaller inertia will yield a high deceleration rate. Consequently, reduced rotor mass improves both accelerating and decelerating capabilities of the motor, which allows fast dynamic performance and better tracking for the desired speed. Section V will present a detailed electromagnetic analysis for the optimized designs.

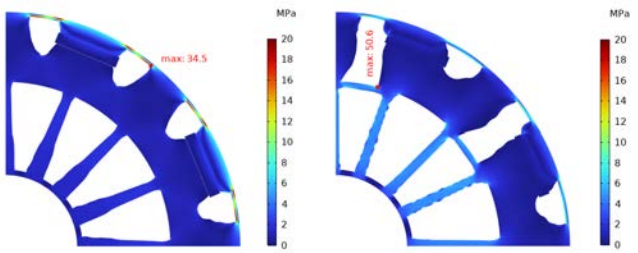

(a) (b)

Fig. 17. The von Mises stress of the optimized designs at 5000 r/min. (a) STO-IPM motor. (b) ATO-IPM motor.

V. Performance Analysis and Comparative Study

To this end, TO design processes for both magnetic and structural stages have been conducted. Then, the optimal design was presented and post-processed. In this part, the performance of four different configurations is investigated and compared. The configurations are the conventional IPM, the modified IPM, the STO-IPM, and the ATO-IPM rotor designs. The performance analysis of the topology-optimized topologies is evaluated after the post-processing stage.

A. No Load Characteristics

To have a clear insight into the topology-optimized IPM configurations and the conventional IPM designs, it is significant to evaluate the airgap magnetic flux distribution. Consequently, the no-load airgap magnetic flux distribution along with its spectrum analysis is presented in Fig. 18. Notably, the fundamental components of the airgap flux density of the topology optimized design are higher than its conventional counterpart by approximately 20%. This increase is attributed to many factors. For ATO-IPM, the first reason is the asymmetric flux barriers, which strengthen the focusing of the flux towards the stator and reduce the leakage flux. Moreover, the TO algorithm removed the rib parts included in the design domain of the magneto-TO. The ribs for topology-optimized designs are the same as those of the modified IPM design, which reduced the saturated parts, as shown in Fig. 19.

Fig. 19 presents the on-load magnetic flux density charts for all IPM topologies. As can be seen, the barriers ATO-IPM reduced the leakage flux. Additionally, the conventional IPM ribs are heavily saturated, which affects the electromagnetic performance. The ATO-IPM design is leading to more efficient utilization of the PMs. The back EMF generated increased in the case of the ATO-IPM design compared to the other topologies, as shown in Fig. 20. It is clear that the fundamental component of the back EMF in the case of the ATO-IPM motor, shown in Fig. 21, is approximately 20% higher than the counterpart of the conventional design at the rated speed. This is certainly because of the improved magnetic flux density through the air gap.

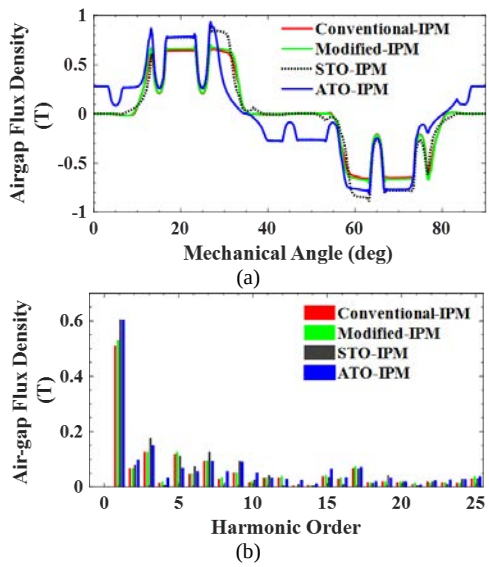

Fig. 18. No load magnetic flux density in the middle of the airgap for both conventional and topology optimized IPM motors. (a) Waveforms. (b) Harmonic components.

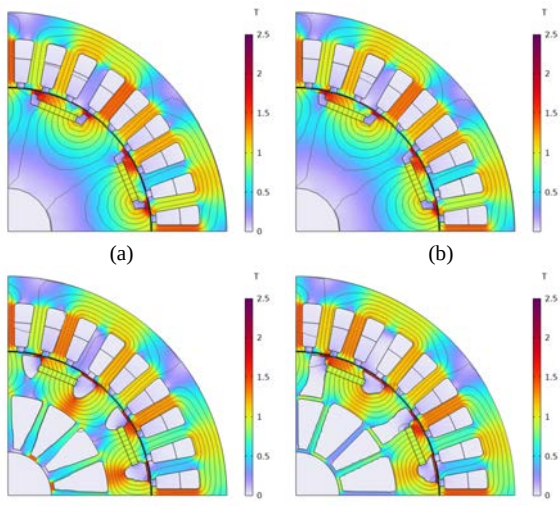

(a) (b)

(c) (d)

Fig. 19. The magnetic flux density distribution charts. (a) Conventional IPM motor. (b) Modified IPM motor. (c) STO-IPM motor. (d) ATO-IPM motor.

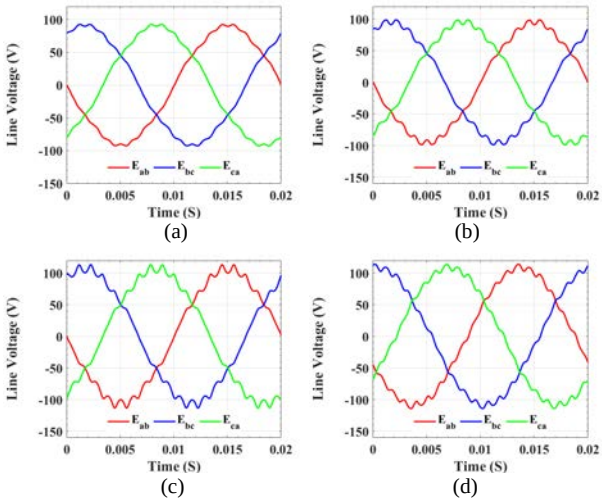

Fig. 20. No load back EMF waveforms. (a) Conventional IPM motor. (b) Modified IPM motor. (c) STO-IPM motor. (d) ATO-IPM motor.

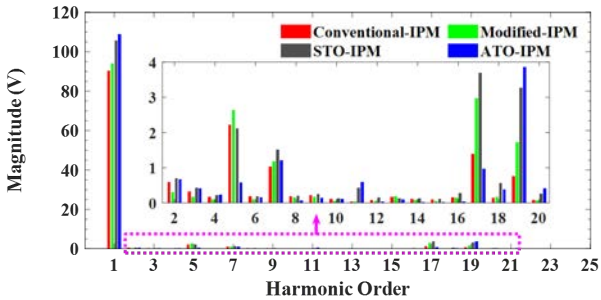

Fig. 21. No load back EMF harmonic order of both topologies.

B. *Torque Analysis*

To gain a deep understanding of differences in developed torque for all topologies, the torque waveforms over one electric period are calculated at rated current, as shown in Fig. 22. The modified IPM shows approximately a 3.5% increase in torque compared to conventional IPM, but the torque ripple also increases. The STO-IPM promises an increase of around 11.6%; however, the torque ripples double compared to the conventional design. In contrast, the proposed ATO-IPM configuration delivers the best torque performance. The average torque increases by 13.3% compared to the conventional design. Moreover, the torque ripple decreases because of the high degree of freedom given to the algorithm to create complete flux lines to maximize the average torque compared to the STO-IPM. Moreover, the spectra analysis of the torque waveforms, shown in Fig. 23, proves that the average torque increases by 13.3% in the case of the ATO-IPM rotor compared to the conventional one. The magnitude of torque harmonics for ATO-IPM also reduces compared to other configurations.

Further analysis for the torque characteristic is depicted in Fig. 24, which presents the instantaneous torque profiles of all designs at rated load. Moreover, the torque profiles are decoupled into two components (PM torque and reluctance torque components), as shown in Fig. 24, for all designs. The torque decoupling was performed by considering freezing the permeability of the core. Now, it is clear that the asymmetric flux barriers developed by the ATO process improved the torque characteristics by improving the alignment of the torque components compared to other configurations. There are two reasons behind this improvement: The first is that the ATO-IPM design reduced the leakage flux and increased the airgap flux. The second reason is the alignment of the torque components. The peaks of the torque components are 45° apart from each other for the STO-IPM, and 30° for both the conventional and modified designs. In contrast, the peaks of the PM torque and reluctance torque components are closer to each other by 20° in case of the ATO-IPM design, as shown in Fig. 24.

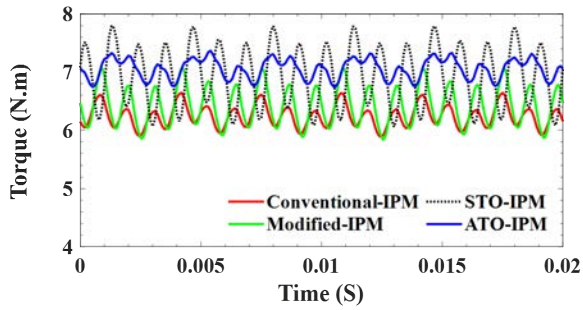

Fig. 22. Developed torque waveforms of the different IPM motor designs.

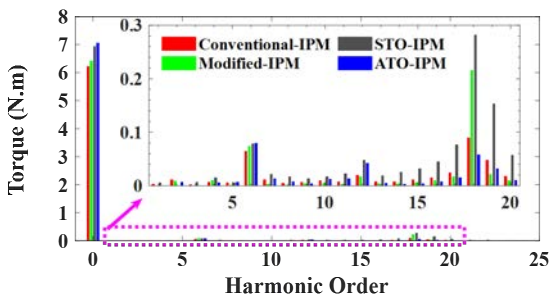

Fig. 23. Harmonic order of developed torque of the different IPM designs.

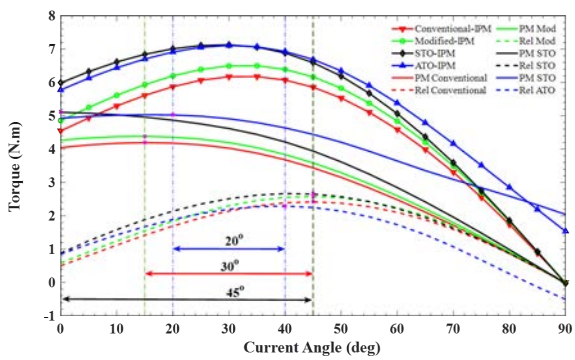

Fig. 24. Instantaneous torque and torque components profiles of the different IPM configurations.

C. *Efficiency and Losses*

In evaluating the performance, it is important to calculate the core losses, output power, and the efficiency of the motor. The losses and efficiency are calculated using FEA based on a periodic time electromagnetic study. The overall losses consist of core losses, copper losses, magnet losses, and mechanical losses. The core losses are approximated using the Bertotti separation method [36] into hysteresis loss, classical eddy current loss, and excess loss, as (8):

$$P_{fe} = k_h f B_m^{\alpha} + k_c f^2 B_m^2 + k_e f^{1.5} B_m^{1.5} \quad (8)$$

where k_h, k_c, and k_e are the hysteresis, classical eddy current, and excess loss coefficients, respectively; f is the supply frequency; B_m is the amplitude of the magnetic flux density; α is the Steinmetz exponent coefficient. The copper loss is calculated as (9):

$$P_{cu} = 3R_s I^2 \quad (9)$$

where R_s is the stator phase resistance, and I is the RMS phase current. Magnet loss and mechanical loss are negligible. Finally, efficiency (η) is calculated as (10):

$$\eta = \frac{P_m}{P_m + P_{fe} + P_{cu}} \quad (10)$$

where P_m is the mechanical output power ($P_m = T_{ave} \cdot \omega$), which is calculated in terms of average torque (T_{ave}) and rotor speed (ω). The core losses P_{fe} are calculated for both stator and rotor.

In this part, the stator core losses, rotor core losses, output power, and the efficiency of the motor are calculated at rated current under different rotation speeds. One of the most notable advantages of the ATO-IPM is the reduction in stator core losses compared to other configurations, shown in Fig. 25(a), which are one of the primary contributors to heat generation and inefficiency in electric machines. At rated speed (750 r/min), the ATO-IPM motor incurs about 33 W of stator core losses, while the conventional design experiences approximately 38 W, amounting to a 13% decrease in these losses. The stator core losses decrease as the ATO-IPM design promises a uniform flux density distribution through the stator core, as shown in Fig. 19. Fig. 25(b) compares the rotor losses for all designs over a range of rotor speeds. As shown, the ATO-IPM and the modified designs consistently exhibit lower core losses than the conventional IPM and STO-IPM designs across the entire speed range from 200 to 1500 r/min.

One of the most notable advantages of the ATO-IPM design is in the mechanical output power compared to other topologies over different rotor speeds, as shown in Fig. 26(a). At rated speed (750 r/min), the ATO-IPM configuration delivers approximately 553 W, outperforming the conventional motor, which provides around 488 W. This corresponds to a 13.3% increase in output power, achieved without any additional input current, highlighting the superior electromagnetic efficiency of the optimized design.

Up to this point, it is clear that the loss reduction and output power improvement will be reflected in the overall efficiency of the motor, as shown in Fig. 26(b). The optimal ATO-IPM motor design achieves an efficiency of approximately 85.4%, which is about 2.4 percentage points higher than the 83% efficiency observed in the conventional motor. This improvement indicates that a greater proportion of the electrical input is effectively converted into useful mechanical work, reducing energy waste. By efficiently shaping the magnetic circuit, the ATO-IPM design enhances not only the performance metrics such as power and efficiency but also contributes to the thermal stability and potential longevity of the motor. Overall, the ATO-IPM clearly demonstrates its effectiveness at medium-speed operation, making it a strong candidate for applications demanding both high efficiency and high-power density.

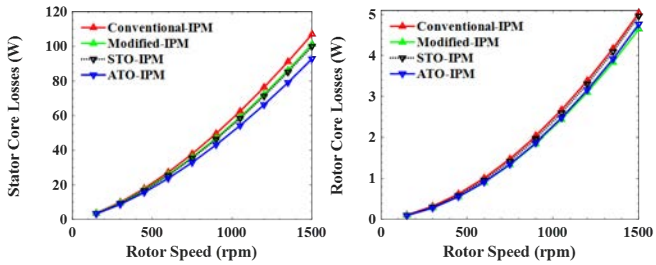

Fig. 25. Stator and rotor core losses of the IPM configurations at rated current and different rotating speeds. (a) Stator core losses. (b) Rotor core losses.

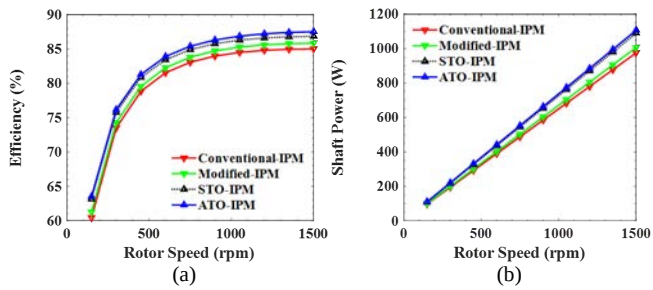

Fig. 26. Output power and efficiency of the IPM configurations at rated current and different rotating speeds. (a) Efficiency. (b) Output power.

D. Influence of Load Variation

In this subsection, the performance of the IPM designs is evaluated under different loading conditions. The load variation analysis is performed from light loads to the rated load. The performance is analyzed, at rated speed, by using FEA based on a periodic time electromagnetic study. As the current increases, the average torque and consequently the output power of all designs linearly increase, as shown in Fig. 27, with the ATO-IPM providing the highest torque and power, indicating improved electromagnetic capability. Furthermore, Fig. 28 presents an increase in both stator and rotor core losses with increasing the load for all configurations, while the ATO-IPM configuration exhibits the lowest core losses. Moreover, the ATO-IPM design achieves the highest efficiency at all loading conditions compared to other designs, as shown in Fig. 29(a). Meanwhile, the power factor decreases as the load increases for all designs, as shown in Fig. 29(b). However, ATO-IPM maintains the highest power factor throughout, reflecting better electrical performance.

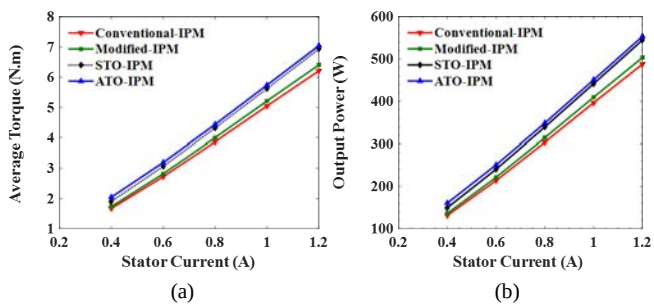

Fig. 27. Average torque and output power of the IPM configurations at rated speed and different stator currents. (a) Average torque. (b) Output power.

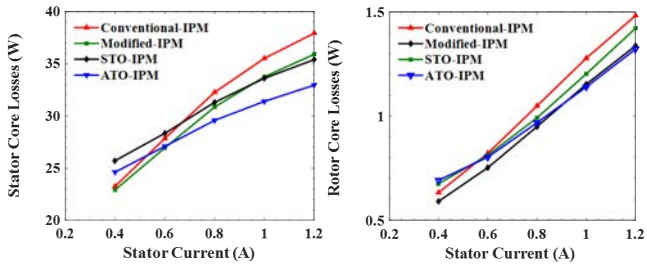

Fig. 28. Stator and rotor core losses of the IPM configurations at rated speed and different stator currents. (a) Stator core losses. (b) Rotor core losses.

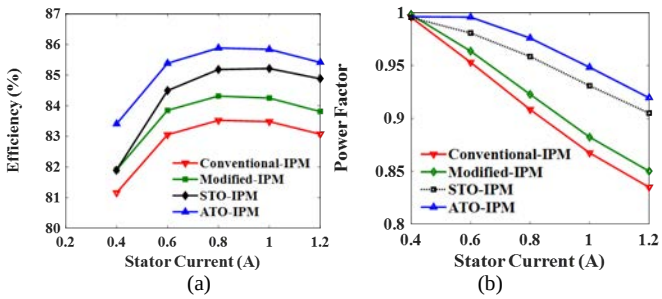

Fig. 29. Efficiency and power factor of the IPM configurations at rated speed and different stator currents. (a) Efficiency. (b) Power factor.

E. Influence of Rotating Direction

Up to this point, the overall performance of the proposed design has been evaluated considering only a single direction of rotation. In all previous results, the reference direction of rotation was anticlockwise. Since the performance of symmetrical designs remains identical regardless of the direction of the rotation, this subsection specifically focuses on evaluating the performance of the asymmetric design in both rotational directions. Before introducing the ATO-IPM motor operating in the reverse direction, it is important to note that the structural TO was carried out based on the results of the magnetic TO, which considered only one direction of rotation. Therefore, the performance of the ATO-IPM design will first be evaluated in both directions for the magnetically topology optimized configuration, before applying the structural TO.

A comparative evaluation of the proposed ATO-IPM machine will be conducted under both directions of rotation. Fig. 30 presents the on-load magnetic flux density distributions, revealing clear direction-dependent behavior due to the ATO-IPM rotor geometry. Under anticlockwise rotation, the flux lines are uniformly distributed, with reduced local saturation in the rotor bridges and stator teeth. In contrast, clockwise operation slightly alters the flux paths and increases localized saturation, resulting in a marginal reduction in torque capability. Fig. 31 presents the torque-current angle characteristics, which further confirm this behavior. The ATO-IPM motor achieves higher peak torque than the conventional IPM in both directions, with the anticlockwise case exhibiting the maximum torque. Moreover, the torque waveforms over one electrical period are calculated at rated current, as presented in Fig. 32. The torque waveforms demonstrate an increased average torque for the ATO-IPM compared to the conventional design. These results verify that the proposed ATO-IPM design enhances torque production but introduces directional performance sensitivity, making the design particularly advantageous for applications with a preferred rotation direction, i.e., fans and compressors.

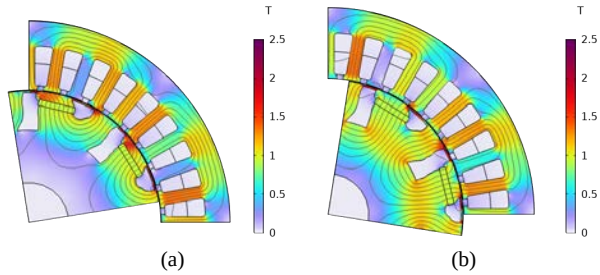

Fig. 30. The on-load magnetic flux density distribution charts of the ATO-IPM motor. (a) Anticlockwise rotation. (b) Clockwise rotation.

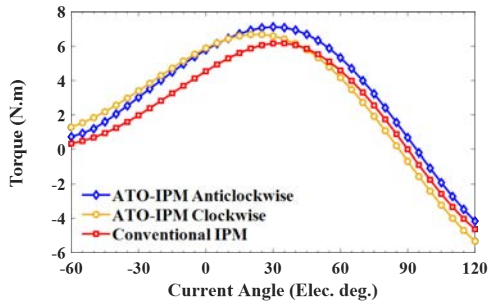

Fig. 31. Comparison of torque-current angle characteristics at different rotation directions.

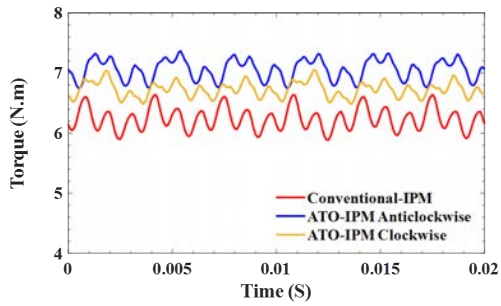

Fig. 32. Torque waveforms of the ATO-IPM machine at different rotation directions.

F. Overall Performance

The overall performance of the ATO-IPM motor is compared with those of the conventional, modified, and STO-IPM designs as illustrated in Table VI. For fair comparison, the conventional design was used as an initial design for the introduced magneto-structural TO process. Moreover, the same stator parameters and PM dimensions were utilized. The performance comparison clearly shows the advantages of applying TO to the IPM rotor design. The STO-IPM design improves torque and power compared to the baseline but suffers from increased torque ripple. In contrast, the ATO-IPM rotor design offers enhanced electromagnetic performance. In this regard, the ATO-IPM design has enhanced torque capability to 7.05 N·m by approximately 13.3% compared to the conventional design. This means efficient utilization for PM as the generated torque is

0.73 (N·m)/cm^3 of PM material in the case of the ATO-IPM design, compared to 0.64 (N·m)/cm^3 of PM material for the conventional design. The optimal design demonstrates an improved output power, developed about 553 W compared to the conventional IPM motor, which yields approximately 488 W while keeping the same PM volume and stator copper losses. Further, the ATO-IPM configuration promises a higher efficiency of 85.41%, surpassing the conventional IPM counterpart, which attains approximately 83.07%. Additionally, both stator and rotor core losses are lower in the case of the ATO-IPM design. Moreover, the rotor mass of the ATO-IPM design is lower than that of the conventional IPM rotor by approximately 46.7%. This demonstrates that the ATO-IPM design, with a high degree of freedom for the TO algorithm, facilitates a more favourable flux path and enhances overall motor performance in comparison with the symmetrical designs.

TABLE VI
OVERALL PERFORMANCE OF THE IPM MOTORS

Item	Conventional IPM (base)	Modified IPM	STO-IPM	ATO-IPM
Average torque/(N·m)	6.21	6.41	6.93	7.05 (↑13.3%)
Torque ripple/%	12.16	19.29	25.09	8.81 (↓3.4%)
Torque/PM vol./((N·m)/cm^3)	0.65	0.68	0.72	0.73 (↑13.3%)
Output power/W	488	503	545	553 (↑13.3%)
Efficiency/%	83.07	83.81	84.90	85.41 (↑2.34%)
Stator core loss/W	37.92	35.91	35.40	32.99 (↓13%)
Rotor core loss/W	1.48	1.34	1.42	1.34 (↓9.4%)
Rotor iron mass/kg	1.840	1.836	1.120	0.980 (↓46.7%)
Power factor	0.835	0.850	0.905	0.920
Rated speed/(r/min)	750	750	750	750
PM vol./cm^3	9.6	9.6	9.6	9.6
Copper loss/W	60	60	60	60

VI. CONCLUSION

This paper presents a novel asymmetric IPM motor designed by employing cascaded magneto-structural TO. The first stage focuses on enhancing electromagnetic characteristics by maximizing average torque while reducing the mass of the magnetically active rotor zone. The second stage addresses mechanical integrity, minimizing the mass of the magnetically inactive rotor region without compromising structural strength. Further, a comparative analysis with conventional and symmetrical topology optimized designs is introduced. The comparative study considering using identical stator and PM parameters confirms the effectiveness of the proposed design. The asymmetric topology optimized design achieves approximately 13.3% higher torque capability, improves torque generation efficiency (0.73 vs. 0.65 (N·m)/cm^3 of PM material), and delivers a higher output power of 553 W compared to 488 W. Moreover, the optimized motor demonstrates superior efficiency (85.4% vs. 83%), reduced core losses, and a substantial 46.7% reduction in rotor mass. These results validate the potential of asymmetric TO to enable more efficient, lightweight, and sustainable IPM motor designs. The ATO-IPM motor exhibits substantial improvements in overall performance compared to the conventional IPM design.

REFERENCES

[1] M. R. Mahmoud, M. N. Ibrahim, and P. Sergeant, "Multi-material Topology Optimization for IPM Machine with Efficient Rare-earth PM Utilization," in *Proc. of IECON 2025 – 51st Annual Conference of the IEEE Industrial Electronics Society*, Madrid, Spain, Oct. 2025, pp. 1–6.

[2] S. Mafrici, V. Madonna, and C. M. Meano *et al*., "Switched Reluctance Machine for Transportation and Eco-design: a Life Cycle Assessment," *IEEE Access*, vol. 12, pp. 68334–68344, May 2024.

[3] H. J. Kim, and D. K. Lim, "Topology Optimization of the IPMSM for HEVs Using a Normalized Gaussian Network with Divided Region Method for Weighting Coefficients," *IEEE Access*, vol. 12, pp. 170677–170687, Nov. 2024.

[4] L. Balasubramanian, N. A. Bhuiyan, and A. Javied *et al*., "Design and Optimization of Interior Permanent Magnet (IPM) Motor for Electric Vehicle Applications," *CES Transactions on Electrical Machines and Systems*, vol. 7, no. 2, pp. 202–209, Jun. 2023.

[5] Y. Ji, Y. X. Li, and Q. F. Lu, "Investigation of a Novel Hybrid Less-rare-earth Consequent-pole Interior Permanent Magnet Machine with Asymmetric Rotor," in *Proc. of 2023 26th International Conference on Electrical Machines and Systems (ICEMS)*, Zhuhai, China, Nov. 2023, pp. 5354–5359.

[6] L. Ding, Y. Cheng, and T. X. Zhao *et al*., "Design and Optimization of an Asymmetric Rotor IPM Motor with High Demagnetization Prevention Capability and Robust Torque Performance," *Energies*, vol. 16, no. 9, pp. 3635, 2023.

[7] Y. Ji, Y. X. Li, and Q. F. Lu, "Novel Asymmetric Rotor Hybrid Interior Permanent Magnet Synchronous Machines for Torque Density and PM Utilization Ratio Improvement," *IEEE Transactions on Industry Applications*, vol. 61, no. 6, pp. 9159–9171, Nov.-Dec. 2025.

[8] Y. Xiao, Z. Q. Zhu, and G. W. Jewell *et al*., "A Novel Asymmetric Rotor Interior Permanent Magnet Machine with Hybrid-layer Permanent Magnets," *IEEE Transactions on Industry Applications*, vol. 57, no. 6, pp. 5993–6006, Nov.-Dec. 2021.

[9] C. W. Diao, W. L. Zhao, and Y. Liu *et al*., "Permanent Magnet Assisted Synchronous Reluctance Motor with Asymmetric Rotor for High Torque Performance," *CES Transactions on Electrical Machines and Systems*, vol. 7, no. 2, pp. 179–186, Jun. 2023.

[10] W. P. Chai, and B. I. Kwon, "Design of an Asymmetric Rotor Pole for Wound Field Synchronous Machines," *CES Transactions on Electrical Machines and Systems*, vol. 5, no. 4, pp. 321–327, Dec. 2021.

[11] F. Tokgoz, Z. Q. Zhu, and X. Chen *et al*., "Novel Hybrid Magnet Asymmetric Rotors for Electric Vehicles," *IEEE Transactions on Transportation Electrification*, vol. 12, no. 2, pp. 3548–3563, Apr. 2026.

[12] Y. Xiao, Z. Q. Zhu, and S. S. Wang *et al*., "A Novel Asymmetric Interior Permanent Magnet Machine for Electric Vehicles," *IEEE Transactions on Energy Conversion*, vol. 36, no. 3, pp. 2404–2415, Sept. 2021.

[13] Z. S. Du, and T. A. Lipo, "Efficient Utilization of Rare Earth Permanent-magnet Materials and Torque Ripple Reduction in Interior Permanent-magnet Machines," *IEEE Transactions on Industry Applications*, vol. 53, no. 4, pp. 3485–3495, Jul.-Aug. 2017.

[14] M. R. Mahmoud, M. N. Ibrahim, and P. Sergeant, "Comprehensive Review on Topology Optimization for Enhancing Electric Machine Performance: Concepts, Methods, Achievements, and Challenges," *IEEE Transactions on Industry Applications*, pp. 1–18, Jan. 2026.

[15] Y. B. Yang, X. H. Wang, and R. Zhang *et al*., "The Optimization of Pole Arc Coefficient to Reduce Cogging Torque in Surface-mounted Permanent Magnet Motors," *IEEE Transactions on Magnetics*, vol. 42, no. 4, pp. 1135–1138, Apr. 2006.

[16] S. N. Xue, and V. Acharya, "Topology Optimization Empowers the Design of Interior Permanent Magnet (IPM) Motors," in *Proc. of 2020 IEEE Transportation Electrification Conference & Expo (ITEC)*, Chicago, IL, USA, Jun. 2020, pp. 1–5.

[17] J. Kwack, S. Min, and J. P. Hong, "Optimal Stator Design of Interior Permanent Magnet Motor to Reduce Torque Ripple Using the Level Set Method," *IEEE Transactions on Magnetics*, vol. 46, no. 6, pp. 2108–2111, Jun. 2010.

[18] Z. Sun, K. Watanebe, and X. Z. Xu, "Derivation of Optimal Rotor

Topologies for Consequent-pole PMSM by ON/OFF Method," *CES Transactions on Electrical Machines and Systems*, vol. 5, no. 4, pp. 301–310, Dec. 2021.

[19] N. Takahashi, T. Yamada, and D. Miyagi, "Examination of Optimal Design of IPM Motor Using ON/OFF Method," *IEEE Transactions on Magnetics*, vol. 46, no. 8, pp. 3149–3152, Aug. 2010.

[20] T. Ishikawa, K. Nakayama, and N. Kurita *et al*., "Optimization of Rotor Topology in PM Synchronous Motors by Genetic Algorithm Considering Cluster of Materials and Cleaning Procedure," *IEEE Transactions on Magnetics*, vol. 50, no. 2, pp. 637–640, Feb. 2014.

[21] J. Q. Wu, B. Tian, and Z. Y. Ren *et al*., "Level Set Method Assisted Topology Optimization of Permanent Magnet Synchronous Machine," in *Proc. of 2023 4th International Symposium on Insulation and Discharge Computation for Power Equipment (IDCOMPU2023)*, Singapore, Jan. 2024, pp. 367–377.

[22] P. Gangl, S. Amstutz, and U. Langer, "Topology Optimization of Electric Motor Using Topological Derivative for Nonlinear Magnetostatics," *IEEE Transactions on Magnetics*, vol. 52, no. 3, pp. 1–4, Mar. 2016.

[23] A. N. A. Hermann, N. Mijatovic, and M. L. Henriksen, "Topology Optimisation of PMSM Rotor for Pump Application," in *Proc. of 2016 XXII International Conference on Electrical Machines (ICEM)*, Lausanne, Switzerland, Sept. 2016, pp. 2119–2125.

[24] Y. S. Hu, Y. Xiao, and B. Chen *et al*., "Topology Optimization of a Consequent-pole Rotor with V-shaped Magnet Placement," in *Proc. of 2018 21st International Conference on Electrical Machines and Systems (ICEMS)*, Jeju, Korea (South), Oct. 2018, pp. 234–239.

[25] H. H. Wu, S. X. Niu, and W. N. Fu, "Optimal Design of Asymmetric Rotor Pole for Interior Permanent Magnet Synchronous Motor Using Topology Optimization," *Energies*, vol. 15, no. 21, pp. 8254, 2022.

[26] T. Cherrière, S. Hlioui, and L. Laurent *et al*., "Topology Optimization of Asymmetric PMSM Rotor," in *Proc. of 2022 International Conference on Electrical Machines (ICEM)*, Valencia, Spain, Sept. 2022, pp. 469–475.

[27] J. Lee, and N. Kikuchi, "Structural Topology Optimization of Electrical Machinery to Maximize Stiffness with Body Force Distribution," *IEEE Transactions on Magnetics*, vol. 46, no. 10, pp. 3790–3794, Oct. 2010.

[28] A. Manninen, J. Keränen, and J. Pippuri-Mäkeläinen *et al.*, "Structural Topology Optimization of High- Speed Permanent Magnet Machine Rotor," in *Proc. of 2020 International Conference on Electrical Machines (ICEM)*, Gothenburg, Sweden, Aug. 2020, pp. 1814–1819.

[29] A. M. Ajamloo, M. N. Ibrahim, and P. Sergeant, "Design Considerations of a New IPM Rotor with Efficient Utilization of PMs Enabled by Additive Manufacturing," *IEEE Access*, vol. 12, pp. 61036–61048, Apr. 2024.

[30] M. Yin, M. Naidjate, and N. Bracikowski *et al*., "Topology Optimization of Non-linear Electromagnetic Actuator based on Reluctance Network Analysis," *Journal of Magnetism and Magnetic Materials*, vol. 602, pp. 172174, Jul. 2024.

[31] Y. Okamoto, Y. Matsubayashi, and S. Wakao *et al*., "Material-density-based Topology Optimization with Magnetic Nonlinearity by Means of Stabilized Sequential Linear Programming: SLPSTAB," *IEEE Transactions on Magnetics*, vol. 51, no. 3, pp. 1–4, Mar. 2015.

[32] M. R. Mahmoud, M. N. Ibrahim, and P. Sergeant, "Evaluating Density-based Topology Optimization Using Different Material Interpolation Schemes: Magnetic Actuator Design Case Study," *Journal of Magnetism and Magnetic Materials*, vol. 636, pp. 173646, Dec. 2025.

[33] A. Kawamoto, T. Matsumori, and S. Yamasaki *et al*., "Heaviside Projection based Topology Optimization by a PDE-filtered Scalar Function," *Structural and Multidisciplinary Optimization*, vol. 44, pp. 19–24, Jul. 2011.

[34] F. Lucchini, R. Torchio, and V. Cirimele *et al*., "Topology Optimization for Electromagnetics: a Survey," *IEEE Access*, vol. 10, pp. 98593–98611, Sept. 2022.

[35] M. R. Mahmoud, M. N. Ibrahim, and P. Sergeant, "Topology Optimization for a Magnetic Actuator Using Different Gradient-based Solvers," in *Proc. of 2025 Joint MMM-Intermag Conference (INTERMAG)*, New Orleans, LA, USA, Jan. 2025, pp. 1–5.

[36] G. Bertotti, "General Properties of Power Losses in Soft Ferromagnetic Materials," *IEEE Transactions on Magnetics*, vol. 24, no. 1, pp. 621–630, Jan. 1988.

Mohamed Reda Mahmoud received the B.Sc. and M.Sc. degrees in electrical and electronic engineering from Minia University, Egypt, in July 2018 and January 2023, respectively. He is currently Ph.D. researcher with the Department of Electromechanical, Systems and Metal Engineering, Ghent University, Gent, Belgium. He has been an assistant lecturer (on leave) in Electrical and Electronic Engineering Department, Mini University, Egypt since February 2023. His research interests include the field of power electronics, motor drives, electric vehicles, topology optimization, analytical modeling of electrical machines and additive manufacturing of electromagnetic components for magnetic actuators and electric machines.

Mohamed N. Ibrahim (Senior Member, IEEE) received the M.Sc. degree in electrical power and machines engineering from Tanta University, Egypt, in November 2012, and the Ph.D. degree in electromechanical engineering from Ghent University, Belgium, in December 2017. He became a Teaching Assistant and an Assistant Professor (on leave) with the Electrical Engineering Department, Kafrelsheikh University, Egypt, in November 2008 and April 2018, respectively. Since December 2017, he has been a Postdoctoral Researcher with the Department of Electromechanical, Systems and Metal Engineering, Ghent University. Since August 2023, he has been an Associate Professor (on leave) with the Electrical Engineering Department, Kafrelsheikh University. He is currently an Affiliate Member of Flanders Make, the strategic research center for the manufacturing industry in Flanders, Belgium. His research interests include electrical machines and drives for sustainability.

Peter Sergeant (Senior Member, IEEE) received the M.Sc. degree in electromechanical engineering and the Ph.D. degree in engineering sciences from Ghent University, Ghent, Belgium, in 2001 and 2006, respectively. In 2006 and 2012, he became a Postdoctoral Researcher and an Associate Professor, respectively. Since 2022, he has been a Full Professor with Ghent University. His research domain is electrical machines and drives for industrial, automotive, and sustainable energy applications. He is an Affiliate Member of Flanders Make, the strategic research center for the manufacturing industry in Flanders. His focus is on accurate modeling, prototyping, and testing of machines and drives, for improving reliability, sustainability, energy efficiency, and power density.